Available online at www.sciencedirect.com
SCIENCE DIRECT®
Thermochimica Acta 425 (2005) 149–163
thermochimica acta
www.elsevier.com/locate/tca

Reliable determination of freeze-concentration using DSC

Bakul S. Bhatnagar[a], Stephane Cardon[a], Michael J. Pikal[a,b], Robin H. Bogner[a,b,*]

[a] *School of Pharmacy, University of Connecticut, U2092, Storrs, CT 06269, USA*
[b] *Institute of Materials Science, University of Connecticut, Storrs, CT 06269, USA*

Received 3 March 2004; received in revised form 22 June 2004; accepted 28 June 2004
Available online 14 August 2004

Abstract

The objective of this study was to determine the feature of a DSC endotherm that can be most reliably used to determine the composition of a freeze-concentrate. Samples (3–10 mg) of sucrose in water (0–60%, w/v) were frozen and then heated (at 0.2–2.0 °C/min) on a DSC. The peak (T_{peak}) and offset (T_{offset}) temperatures were obtained from the melt endotherms. A freezing point osmometer was also used to determine the freezing point depression of sucrose solutions. Two theoretical models were developed, one that describes melting in a one-component system (ice) with a heterogeneous temperature distribution, and a second model, which describes melting in a binary system (sucrose and ice) with a homogeneous temperature distribution. Modeling Laboratory (MLAB) was used to simulate melt endotherms using the two models. In Gray's theory for analysis of dynamic thermal measurement (1968), the end of the melting occurs at the peak of the endotherm followed by a much sharper recovery to the baseline than that observed experimentally. Our theoretical model for one- and two-component systems predicts that the melting continues beyond the peak resulting in a delayed recovery to the baseline as experimentally observed. Both experimental and simulated T_{peak} and T_{offset} (also defined as the return to the baseline after completion of the peak) increased with an increasing scan rate. Extrapolation of the experimental T_{offset} to a zero scan rate yielded a value of the equilibrium melting temperature, T_m, which is closer to accepted literature values and osmometry data than did the extrapolation of T_{peak}. Neither T_{peak} nor T_{offset} reliably (at a finite scan rate) define the multicomponent freezing point. Rather, an extrapolation of T_{offset} to a zero scan rate gives the most reliable measure of freezing point using DSC. Simulation of DSC endotherms supports this conclusion and also exhibits the same trends as observed from experiment.

Keywords: Sucrose; DSC; Freeze-concentration; T_{offset}; Ice melting

1. Introduction

Freeze-drying is the process of choice to stabilize many parenteral antibiotics, peptides and proteins [1]. Ice formation during the freezing step in a freeze-drying process results in the increase in concentration of the dissolved solutes. This process, known as freeze-concentration, may lead to changes in pH, aggregation, phase separation, and other destabilizing processes [2]. To better understand the destabilizing mechanisms that occur during freeze-concentration, the composition of the freeze-concentrate must be well-defined at all relevant temperatures. The composition of the freeze-concentrate for a formulation can be calculated from the equilibrium liquidus curve of the phase diagram if known. To resolve the effect of pure freeze-concentration on stability of frozen protein or antibiotic solutions, one can study the isothermal degradation kinetics of unfrozen formulations of a concentration same as that of the freeze-concentrate as defined by the liquidus curve. Thus, an accurate determination of the freeze-concentrate has significant implications in the study of the stability of frozen proteins and antibiotics during freeze-drying.

Glucose, sucrose, trehalose, and other sugars are widely used as bulking agents and stabilizers in lyophilized formulations. The universal quasi-chemical (UNIQUAC) [3] and universal functional activity coefficient (UNIFAC) [4] models have been utilized to predict freezing points of binary

* Corresponding author. Tel.: +1 860 486 2136; fax: +1 860 486 4998.
E-mail address: robin.bogner@uconn.edu (R.H. Bogner).

0040-6031/$ – see front matter © 2004 Elsevier B.V. All rights reserved.
doi:10.1016/j.tca.2004.06.017

Nomenclature

dh/dt	heat generated by the sample during melting
Δh_0	heat of fusion of ice present in the DSC sample
ΔH_f	heat of fusion of ice per gram
$(dQ/dt)_r$	heat flow to the reference during melting
$(dQ/dt)_s$	heat flow to the sample during melting
dT_r/dt	scan rate or heating rate, S
dT_s/dt	rate of change of sample temperature with time
ΔT_f	freezing point depression
ΔT_{melt}	difference between T_{offset} and T_{onset} for pure water
a_1	coefficient 1 for the binary system in Eq. (17) and is used in fitting of the model to describe DSC data
a_2	coefficient 2 for the binary system in Eq. (17) and is used in fitting of the model to describe DSC data
A_{00}	parameter in evaluation of area, $A(z)$
A_{01}	parameter in evaluation of area, $A(z)$
$A(z)$	area of the ice:water interface in the HTD model
C	constant in $z(m)$ empirical equation
C_2	constant in $z(m)$ empirical equation
C_{ice}	heat capacity of ice
$\bar{C}_p^l$	specific heat of water
C_r	heat capacity of the reference pan
C_s	sample heat capacity (includes heat capacity of the sample pan)
$C_w(m)$	effective heat capacity of water
C_w^0	initial value of C_w
h	height of ice sample in sample pan assuming a cylindrical geometry in the HTD model
$\bar{H}_1^0$	partial molal enthalpy of water before dilution of the freeze-concentrate
$\bar{H}_1(m')$	partial molal enthalpy of water after dilution of the freeze-concentrate where the new composition of the freeze-concentrate is m'
k	thermal conductivity of water
K_f	cryoscopic constant
m_0	mass of the ice sample in the HTD model
m	mass of water
m_{onset}	molality of the maximal freeze-concentrate
$m_{solution}$	molality of a solution in Eq. (2)
n_1	number of moles of solvent (water)
n_2	number of moles of solute
n_m	number of moles of water in the freeze-concentrate following dilution
r	radius of ice sample in sample pan assuming a cylindrical geometry in the HTD model
R	thermal resistance and is same as total thermal resistance, R_T which is a sum of R_0 and $R_s(m)$ used in the one-component model
R_0	thermal resistance across the DSC:aluminum pan interface
$R_s(m)$	sample thermal resistance
S	scan rate (heating rate)
T_f	furnace temperature
T_l	mean temperature of water in Eq. (24)
T_{melt}	temperature of melt end = $T_{onset} + St$
T_r	reference pan temperature
T_{r_0}	reference pan temperature at time zero, i.e., start of the scan
T_s	sample pan temperature
T_0	freezing point of pure water
T_m	freezing point of a solution of molality (m)
T_{onset}	onset melting temperature in a two- (or a multi-) component system
T_z	ice temperature
$\bar{X}_2^0$	mole fraction in the freeze-concentrate before the onset of melting in the incorporation of the heat of dilution effect in Eq. (14)
$\bar{X}_2^F$	mole fraction in the freeze-concentrate after all ice is melted in the incorporation of the heat of dilution effect in Eq. (14)
z	thickness of the water layer surrounding ice in Fig. 1
$Z_s(m)$	derivative of R_s with respect to m, dR_s/dm

sugar–water systems. Another model based on solute/solvent interaction corrections was used to account for non-ideal freezing point depression and extend freezing point depression theory to the high concentration range [5]. Even though such models are useful for defining the liquidus curve of simple carbohydrate–water systems, they are less useful for studying pharmaceutical systems, which are compositionally more complex.

Prior to the development of calorimetric techniques, the liquidus curve was constructed by careful visual observation of the end of melting [6]. Such measurements were often very slow and tedious. The freezing point depression for aqueous solutions of carbohydrates and/or other solutes reported in the widely used International Critical Tables are based on such traditional measurements performed in the late 19th and early 20th centuries [7–9], and are cited routinely in the thermal literature even today [10]. With the development of other methods such as osmometry, refractometry [11], DTA [12–14], and DSC [15,16], freezing point determination has become easier and faster.

Today DSC has, in fact, become the method of choice for the determination of freezing point depression and for the construction of the liquidus curve of the phase diagram

[15–19]. Blond et al. used the peak temperature to define the melting temperature [16]. Ablett et al. [15] and Wang and Haymet [17] determined the peak temperature at several heating rates and extrapolated the peak temperature to a zero heating rate. Tan and Man determined the offset (also defined as the return to the baseline) after melting at several heating rates and extrapolated the offset temperature to zero heating rate to distinguish between vegetable oil products [19]. None of the authors justified the use of T_{peak} or T_{offset}, nor the extrapolation to a zero heating rate as the accurate marker for the end of melting. For the purposes of constructing an accurate phase diagram from which one can calculate a reliable value for freeze-concentration, the true end of melting must be clearly defined. The determination of the concentration of the maximal freeze-concentrate, C_g', and its glass transition temperature, T_g', have been the focus of several published reports [15,20–23]. In contrast, the focus of our work is to characterize the equilibrium freeze-concentrate well above the T_g' where the glass:crystalline interface is not a complicating factor.

Several attempts have been made to better understand and define the features of the DSC peak in a melt endotherm [24–27]. Work on melting in one-component systems has been largely based upon the model proposed by Gray [28]. Gray's theory for melting in a DSC assumes uniform melting and therefore, homogeneous sample temperature throughout the melting process. An important result of this model is that melting is completed at the peak followed by an almost instantaneous recovery to the baseline, a phenomenon that is not observed experimentally. Popa and Segal analyzed the DSC melt endotherms of pure ice using functions traditionally employed in spectroscopic and chromatographic signal processing to describe peak broadening and shape differences due to varying heating rate and sample mass [24]. Their results document a peak broadening and shift in T_{peak} with both increasing heating rate (1–5 °C/min) and increasing sample mass (1.8–10.8 mg). While their treatment is somewhat empirical, the authors convincingly discuss the analogy of increasing sample mass in a DSC sample pan to sample load on a chromatographic column. Thermal lag is identified as the cause for both peak broadening and shift.

Wang and Harrison explored the effect of thermal lag by mixing polyethylene with indium to increase the thermal lag during the melting of indium, which resulted in peak broadening and peak shift [25,27]. These results again implicate the thermal lag as a key determinant of peak shape that was missing from Gray's original theory. Further, Wang and Harrison modeled the thermal lag by treating the sample as a series of shells, each with a resistance and heat capacity that varied linearly with distance from the sample surface to it's interior [26]. The simulated melt endotherms were generated by summation of the melting of successive shells each modeled using Gray's theory. The simulated endotherms were similar in peak shape and temperature to the experimentally generated melting curve. Each of these studies attempted to quantify the effect of the thermal lag on the peak temperature and peak shape. However, none have attempted to determine the relationship of the peak temperature or other endotherm feature to the true end of melting, the feature needed to define a freeze-concentrate.

The objectives of the present study were to model the effect of a solute on the DSC endotherm and to model melting of a one-component system in a DSC pan without Gray's simplifying assumption of a homogeneous temperature. An attempt was made to identify the feature of the DSC thermogram that best correlates with the end of the melt and use that feature to construct a phase diagram for sucrose in water to define the composition of the freeze-concentrate.

2. Experimental

Crystalline sucrose of analytical grade was used as received (Lot #98H03291) (Sigma Chemical Co., St. Louis, MO, USA). Distilled, deionized water was used for preparation of sucrose solutions. A differential scanning calorimeter (2920 Modulated DSC, TA Instruments, New Castle, DE, USA) in the standard mode and equipped with a refrigerated cooling system (TA Instruments, New Castle, DE, USA) was employed for this study. A Universal Analysis Program (Version 1.11A, TA Instruments, New Castle, DE) was used for monitoring and processing heat flow-temperature curves. Aluminum sample pans (TA Instruments, New Castle, DE, USA) were used for holding the sample during the DSC runs. Prior to use in the experiment, the aluminum pans were cleaned with methanol and sonicated in methylene chloride for 15 min to remove coatings, if any, on the pans and air dried. Using this procedure, it was easier to spread the sample solution evenly on the pan surface as a thin film and ensure a good thermal contact with the pan.

Solutions of sucrose in water (10–60%, w/v) were prepared at room temperature. Samples (3–10 mg) were transferred to aluminum DSC pans using a 25 μL microsyringe and spread as a film using tweezers, and sealed hermetically. Nitrogen gas (flow rate, 50 mL/min) was used for the cell purge, and helium (flow rate, 150 mL/min) was used for the refrigerated cooling system. The DSC was calibrated at 2 °C/min using indium and water as standards. All samples were cooled to −50 °C at a rate of 5 °C/min and heated at programmed rates (0.2–2.0 °C/min). In addition, a freezing point osmometer (3MO Plus Advanced Micro-Osmometer, Advanced Instruments, Inc., Norwood, MA, USA) was used to determine the freezing point depression of sucrose solutions.

MLAB software (Modeling Laboratory, Civilized Software, Bethesda, MD, USA) was used to simulate endotherms according to the models developed below. Comparisons of the simulations with the experimental thermograms were used to identify the endotherm feature that best represents the end of melting.

3. Theory

3.1. Extension of Gray's theory to multicomponent systems

Based on the principle of operation of a heat flux DSC, Gray [28] developed an expression for the DSC power required during melting of a sample,

$$\frac{dh}{dt} = \frac{T_s - T_r}{R} + (C_s - C_r)\frac{dT_r}{dt} + C_s\frac{d(T_s - T_r)}{dt} \quad (1)$$

where dh/dt is the heat generated by the sample during melting, R is the thermal resistance, T_s is the sample temperature, T_r is the reference temperature, C_s is the heat capacity of the sample, C_r is the heat capacity of the reference, and, dT_r/dt is the scan rate. The term $(T_s - T_r)/R$ corresponds to DSC power. Gray's theory assumes that the sample temperature remains constant and uniform during melting. However, in a multicomponent system, the melting point increases as melting proceeds and lowers the solute concentration in the liquid. The effect of the time dependence of the melting point on the shape of the endotherm is evaluated here by modifying Gray's theory. In the initial development of the model, the heat of dilution is assumed to be negligible.

We further assume that the ideal solution relationship is valid.

$$\Delta T_f = T_0 - T_m = K_f m_{solution} \quad (2)$$

where $m_{solution} = n_2 \times 1000/w$ is the molality of the solution, T_0 is the freezing point of pure water, T_m is the freezing point of a solution at a molality, $m_{solution}$, K_f is the cryoscopic constant, n_2 is the number of moles of solute, and w is the mass of water. During melting, the sample temperature in Eq. (1), T_s, is equal to T_m in Eq. (2). The rate of change of T_m (or T_s) with time is described in terms of the rate of change of the mass of water, w, with time.

$$\frac{dT_s}{dt} = (T_0 - T_s)\frac{d\ln w}{dt} \quad (3)$$

Also,

$$\frac{dh}{dt} = -\Delta H_f\frac{dw}{dt} \quad (4)$$

where ΔH_f is the heat of fusion of ice.

Combination of Eqs. (2)–(4) yields,

$$\frac{dh}{dt} = \frac{K}{(T_0 - T_s)^2}\frac{dT_s}{dt} \quad (5)$$

where

$$K = \Delta H_f K_f n_2 \times 1000$$

In the formulation of the model, it was assumed that the melting starts at $t = 0$. The temperature corresponding to $t = 0$ is T_{onset} and is determined by

$$\Delta T_f = T_0 - T_{onset} = K_f m_{onset} \quad (6)$$

where m_{onset} represents the molality of the maximal freeze-concentrate, and T_{onset} represents the onset of melting in a two- (or a multi-) component system and is determined by the freezing point depression of the freeze-concentrate. Assuming that the freeze-concentrate contains 18% water [22,23], the concentration of sucrose in the freeze-concentrate is calculated to be 13.3m. Using Eq. (6) with $K_f = 1.9$, the value of T_{onset} was determined to be approximately −25 °C.

The integral of dh over all t yields the total heat of fusion of the ice present, Δh_0. Therefore, Eq. (1) is integrated and rearranged to provide an equation,

$$\Delta h_0 = (C_s - C_r)St_{melt} + C_s[(T_s - T_r)_{t_{melt}} - (C_s - C_r)_{t_0}] + \frac{1}{R}\int_{t_0}^{t_{melt}} (T_s - T_r)\,dt \quad (7)$$

where S is the scan rate, dT_r/dt.

In addition, equating (1) and (5) yields,

$$-\frac{dT_s}{dt} = \frac{(T_0 - T_s)^2}{[K + C_s(T_0 - T_s)^2]}\left(\frac{T_s - T_r}{R} - C_r S\right) \quad (8)$$

Eqs. (7) and (8) are solved simultaneously to obtain the time, t_{melt}, at which melting is complete in a two-component system. The simulation involves an energy balance where the T_{melt} is the temperature at which the calculated Δh_0 from Eq. (7) becomes equal to the known value of Δh_0, and determines the end of melting. Further, numerical integration of Eq. (8) as a function of time yields DSC power, $(T_s - T_r)/R$, versus time from t_0 to t_{melt}, the time at which melting is complete.

Prior to the onset of melting and after the end of melting, $dh/dt = 0$, and Eq. (1) becomes,

$$\frac{d(T_s - T_r)}{dt} = -\frac{T_s - T_r}{RC_s} - S\left(1 - \frac{C_r}{C_s}\right) \quad (9)$$

Eq. (9) is used to describe the time dependence of $(T_s - T_r)$ before the onset of melting and after the end of melting.

From Eqs. (8) and (9), the DSC power curves for frozen sucrose:water solutions can be obtained as a function of time. Power curves as a function of temperature are obtained from the scan rate, which relates time, t, to temperature, T.

3.1.1. Estimation of thermal resistance using pure water

For a one-component system, the end of melting, t_m, can be obtained from Eq. (1) by integration of dh from $t = t_0$ to $t = t_m$ to obtain the value for heat of fusion, Δh_0, which can also be calculated from the knowledge of total mass of ice and ΔH_f (heat of fusion of ice). Knowing the scan rate, S, the temperature at which the last crystal of ice melts, T_{melt}, is obtained using, $T_{melt} = T_{onset} + St$. The value of $(T_s - T_r)_0$ is required in the integration of Eq. (1). At time zero, melting has not yet begun; therefore dh/dt and $d(T_s - T_r)/dt$ in Eq. (1) are zero, which yields,

$$(T_s - T_r)_0 = -RS(C_s - C_r) \quad (10)$$

The values of S, C_s and C_r are known. However, one must calibrate for thermal resistance, R, which is accomplished by

analyzing melt data for pure water. Eq. (1) can be rewritten for pure water where $T_s = T_0$, and $dT_s/dt = 0$. Integration of the resulting equation from the onset of ice melt, $t = t_0$ (or $T_{onset} = 0\,^{\circ}C$), to the end of melting, $t = t_m$ (or T_{melt}) followed by solving for R yields,

$$R = -\frac{\Delta T_{melt}^2}{2S(\Delta h_0 + C_s\,\Delta T_{melt})} \tag{11}$$

where ΔT_{melt} is the difference between T_{offset} and T_{onset} for pure water. Since the value of R should be the same for multi-component systems as for pure water, the value of R calculated from Eq. (11) was substituted in Eqs. (7)–(9) to determine T_{melt} and generate the DSC power curve for frozen sucrose:water solutions.

3.1.2. Incorporation of the heat of dilution effect

In the preliminary development of the model, we assumed that the contribution of the heat of dilution to the total heat generation is negligible. The purpose of this subsection is to develop equations to account for the effect of the heat of dilution on the shape of the melt endotherm. We evaluate the melting of ice to form water, which then dilutes the freeze-concentrate. In this discussion, n_1 and n_2 represent moles of water in the freeze-concentrate and the solute, respectively. As stated earlier, heat generation occurs in two steps,

(1) melting of ice to form dn_1 moles of water, where the differential heat is,

$$dH_{melt} = \Delta H_f\,dn_1, \text{ and} \tag{12}$$

(2) dilution of the freeze-concentrate by dn_1 moles of water where the new composition of the freeze-concentrate is m'. Using the Gibbs–Duhem equation, the differential heat requirement is

$$dH_{dil} = dn_1(\bar{H}_1(m') - \bar{H}_1^0) \tag{13}$$

where $\bar{H}_1^0$ and $\bar{H}_1(m')$ represent the partial molal enthalpies of the dn_1 moles of water before and after the dilution of the freeze-concentrate, respectively.

The total heat generated, dH, is the sum of dH_{melt} and dH_{dil}. Dividing dH by dn_1 yields

$$\frac{dH}{dn_1} = \Delta H_f + (\bar{H}_1(m') - \bar{H}_1^0) \tag{14}$$

The difference in partial molal enthalpies in Eq. (14) can be determined from the total heat absorbed in melting a series of frozen solutions at various solute concentrations as described below.

Eq. (14) is integrated over the range of ice melting between the limits 0 and n_m, where n_m represents the maximum number of moles of water generated by ice melting in the freeze-concentrate following dilution. Further, the concentration units are converted from molality, m, to mole fraction, X noting that when $n_m = 0$, $X_2 = X_2^0$, the mole fraction in the freeze-concentrate before the onset of melting. Therefore, Eq. (14) becomes

$$\frac{\Delta H}{n_m} = \Delta H_f + \left(\frac{X_2^F}{X_1^F}\right)\int_{X_2^F}^{X_2^0} \frac{(\bar{H}_1^0 - \bar{H}_1(X_2))}{X_2^2}\,dX_2 \tag{15}$$

where the notation "F" refers to the final state when all ice is melted. Rearranging Eq. (15), we define Y

$$Y = \left(\frac{X_2}{X_1}\right)\left(\Delta H_f - \frac{\Delta H}{n_m}\right) = \int_{X_2^F}^{X_2^0} \frac{(\bar{H}_1^0 - \bar{H}_1(X_2))}{X_2^2}\,dX_2 \tag{16}$$

Differentiating Y with respect to dX_2^F yields

$$\frac{dY}{dX_2^F} = -\frac{(\bar{H}_1^0 - \bar{H}_1(X_2^F))}{(X_2^F)^2} \tag{17}$$

From experimental DSC data for the heat of melting of various frozen sucrose:water solutions, Y is evaluated as a function of X_2^F and numerically differentiated. That is, ΔH is the area of the ice melt endotherm where n_m moles of ice melt and X_2^F is the concentration of the final solution thus formed. An empirical function

$$-\frac{dY}{dX_2^F} = \frac{a_1}{(1 + a_2 X_2^F)^2} \tag{18}$$

was found to give a good fit to the experimental data where a_1 and a_2 are coefficients determined by a fit of Eq. (18) to the data.

The contribution of the effect of heat of dilution on the total heat generated in the melting of ice, dH/dn_i, is obtained from manipulation of Eqs. (14), (16)–(18) to give,

$$\frac{dH}{dn_i} = \Delta H_f - \frac{a_1 X_2^2}{(1 + a_2 X_2)^2} \tag{19}$$

To include the heat of dilution modification in the preliminary model, the term K in Eq. (5) is now expressed as a function of the independent variable, X_2,

$$K(X_2) = K_f n_2 \times 1000\left(\Delta H_f - \frac{a_1 X_2^2}{1 + a_2 X_2^2}\right) \tag{20}$$

Eq. (20) includes the effect of heat of dilution on the total heat generated during melting and may be used to simulate the DSC power curves for frozen sucrose solutions as a function of time or temperature as described by Eqs. (7) and (8), except now the term K is not a constant.

3.2. Extension of Gray's theory to a heterogeneous sample temperature distribution

Gray's theory for melting in one-component systems assumes uniform sample temperature during melting, which

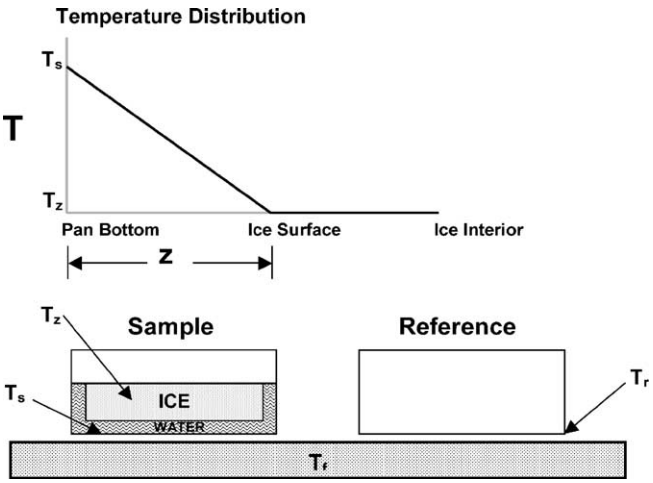

Fig. 1. Schematic of the DSC reference pan and the sample pan where, T_r is the reference pan temperature, T_s is the sample pan temperature, T_z is the ice temperature, and z is the thickness of the water layer surrounding the ice.

yields the result of the end of melting occurring at the peak of the melt endotherm. Gray's theory also shows that the signal decay in DSC power toward the baseline from the peak occurs so rapidly that the extrapolated offset temperature of the melt endotherm differs only slightly from the endotherm peak. However, experimentally one observes that the decrease to the baseline is much slower than predicted from Gray's theory. We hypothesize that the difference between theory and experiment is due to a temperature gradient that exists across the sample. In addition, we hypothesize that as the ice melts from both the bottom and the sides of the original ice mass in a DSC pan, the ice:water interfacial area decreases.

The objective of this section is to evaluate the temperature at which melting is complete in a one-component system where a temperature gradient and contracting sample geometry are built into the model. The model is confined to a one-component system to keep the treatment simple. Fig. 1 shows a schematic of a sample of water and a reference pan in a heat-flux DSC. It is assumed that the ice sample contacts the aluminum pan only at the bottom and the sides of the pan. Thus, melting proceeds from the bottom and the sides of the pan. The thickness of the water layer surrounding the ice, denoted z, increases as melting proceeds (Fig. 1). As ice melting occurs, it is assumed that the temperature profile over distance within the water layer is linear, while the temperature of the ice is assumed to be a constant, T_z (Fig. 1).

As in Gray's theory, heat flow to the reference pan, $(dQ/dT)_r$, can be described as

$$\left(\frac{dQ}{dt}\right)_r = \frac{T_f - T_r}{R_0} = C_r \frac{dT_r}{dt} \tag{21}$$

where T_f is the DSC furnace temperature, T_r is the reference pan temperature, R_0 is the thermal resistance from the DSC furnace to the pan:sample interface, C_r is the heat capacity of the pan and dT_r/dt is the scan rate.

Similarly, the heat flow to the sample, $(dQ/dt)_s$, may be written as

$$\left(\frac{dQ}{dt}\right)_s = \frac{T_f - T_s}{R_0} \tag{22}$$

where T_f is the DSC furnace temperature, T_s is the sample pan temperature, and R_0 is the thermal resistance from the DSC furnace to the pan:sample interface.

Heat flow to the sample, $(dQ/dT)_s$ as long as some water is present, can also be expressed as

$$\left(\frac{dQ}{dt}\right)_s = \frac{T_s - T_z}{R_s} \tag{23}$$

where T_z is the ice temperature and R_s is the thermal resistance across the water layer in the sample.

Assuming that the ice temperature remains constant during melting and that both the pan and water temperatures increase as the furnace temperature increases, heat flow to the sample during melting can be written as

$$\left(\frac{dQ}{dt}\right)_s = \Delta H_f \frac{dm}{dt} + mC_p^l \frac{dT_l}{dt} + C_r \frac{dT_s}{dt} \tag{24}$$

where C_p^l is the specific heat of water, m is the mass of water, and C_r is the heat capacity of the DSC pan. The first term on the right hand side represents the heat flow for melting of ice, and the second and third terms are heat capacity terms for the water and the pan, respectively. Since a linear temperature profile with distance over the water layer is assumed, the mean temperature of the water, T_l, is $(T_z + T_s)/2$. With T_z constant, $dT_l/dt = (dT_s/dt)/2$. Thus, $mC_p^l\, dT_l/dt$ in Eq. (24) becomes $(m/2)C_p^l\, dT_s/dt$.

The DSC power, $(T_s - T_r)/R_0$, is obtained from subtraction of Eq. (24) from Eq. (21) to obtain,

$$-\frac{T_s - T_r}{R_0} = \Delta H_f \frac{dm}{dt} + (C_w(m) + C_r)\frac{d(T_s - T_r)}{dt} + C_w(m)S \tag{25}$$

where $C_w(m)$ is substituted for $(m/2)C_p^l$.

Eq. (25) is a differential equation in two dependent variables, $(T_s - T_r)$ and m, with independent variable, t. With an equation for dm/dt the system can be completely defined. To obtain the needed expression, Eq. (22) is set equal to Eq. (23), and differentiated with respect to time to obtain

$$\frac{dT_s}{dt} + \frac{R_s}{R_0}\frac{dT_s}{dt} + \frac{T_s}{R_0}\frac{dR_s}{dt} = \frac{dT_z}{dt} + \frac{R_s}{R_0}\frac{dT_f}{dt} + \frac{T_f}{R_0}\frac{dR_s}{dt} \tag{26}$$

where

$$\frac{dR_s}{dt} = \frac{dR_s}{dm}\frac{dm}{dt} = Z_s(m)\frac{dm}{dt} \tag{27}$$

in which $Z_s(m)$ represents the derivative of R_s with respect to m. A detailed discussion on the determination of R_s as a function of mass of ice melted is included in a later Section

3.2.1. Recognizing that $dT_f/dt = dT_r/dt = S$ and $d(T_s - T_r)/dt = dT_s/dt - S$, we substitute Eq. (27) into Eq. (26) to obtain

$$\frac{dm}{dt} = \frac{(R_0 + R_s(m))}{(T_f - T_s)Z_s(m)}\frac{d(T_s - T_r)}{dt} + \frac{R_0 S}{(T_f - T_s)Z_s(m)} \quad (28)$$

Rearranging Eq. (21) yields $T_f - T_s = R_0 C_r S - (T_s - T_r)$ which is substituted into Eq. (28) to obtain

$$\left(\frac{dm}{dt}\right) = \frac{(R_0 + R_s(m))}{Z_s(m)[R_0 C_r S - (T_s - T_r)]}\frac{d(T_s - T_r)}{dt} + \frac{R_0 S}{Z_s(m)[R_0 C_r S - (T_s - T_r)]} \quad (29)$$

At any temperature, T_r, the amount of ice melted, m, is obtained by integration of Eq. (29). At the end of the ice melt, the value of m is denoted, m_0, which is the initial mass of ice. In the MLAB program, values of $m(T)$ are generated in the solution of the differential equations, and the value of T_{melt} is the temperature as which m becomes equal to m_0. Further, substitution of Eq. (29) into Eq. (25) with rearrangement yields

$$\frac{d(T_s - T_r)}{dt} = -\frac{[(T_s - T_r)/R_0 S + C_w(m)S + \Delta H_f R_0 S/Z_s(m)(R_0 C_r S - (T_s - T_r))]}{[C_r + C_w(m) + \Delta H_f(R_0 + R_s)/Z_s(m)(R_0 C_r S - (T_s - T_r))]} \quad (30)$$

with the initial condition: $(T_s - T_r)_0 = -R_0 C_{ice} S$ where C_{ice} is the heat capacity of ice. Eq. (30) applies when $0 \le t \le t_{melt}$ (or when $0 \le m \le m_0$) where t_{melt} is the time at which melting is complete as determined by the integration of Eq. (29).

After the completion of melting, $dm/dt = 0$, $m = m_0$, $C_w = C_w^0$, and Eq. (25) becomes,

$$\frac{d(T_s - T_r)}{dt} = -\frac{T_s - T_r}{R_0(C_w^0 + C_r)} - \frac{C_w^0 S}{C_w^0 + C_r} \quad (31)$$

The DSC power curves for one-component samples can be obtained as a function of time by integration of Eqs. (30) and (31). DSC thermograms as a function of temperature are obtained by using scan rate to transform time, t, to temperature, T.

3.2.1. Determination of R_s as a function of m

The model was further refined to determine R_s as a function of the amount of ice melted. Assuming a contracting cylindrical geometry for the ice, the heat transfer rate to the sample, $(dQ/dt)_s$ was determined in terms of the temperature gradient, $(T_s - T_z)/z$, the area of the ice:water interface, $A(z)$, and the thermal conductivity of water, k, using the relationship,

$$\left(\frac{dQ}{dt}\right)_s = A(z)k\frac{T_s - T_z}{z} = \frac{T_s - T_z}{R_s} \quad (32)$$

Therefore,

$$R_s = \frac{z}{kA(z)} \quad (33)$$

The area, $A(z)$ is evaluated in terms of the height, h and the radius, r of the ice cylinder.

$$A(z) = \pi r_0^2\left(1 - \frac{z}{r_0}\right)^2 + 2\pi r_0 h_0\left(1 - \frac{z}{r_0}\right)\left(1 - \frac{z}{h_0}\right) \quad (34)$$

The thickness of the water sample, z, was related to the mass of water, m, by approximating the water volume as the difference between the initial sample volume and the volume of residual ice. The approximation is not exact as the densities of ice and water differ. However, for the purpose of keeping the model development simple at this point, it seems reasonable to make the assumption. In general, since the initial sample height is less than the sample radius, the value of z/r_0 is less than unity at the end of melting. Thus, assuming equal densities for ice and water, the relationship between m and z is

$$1 - \left[1 - \frac{z}{r_0}\right]^2\left[1 - \frac{z}{h_0}\right] - \frac{m}{m_0} = 0 \quad (35)$$

where z is given by the positive roots of Eq. (35) for various values of m. The shape of the function $z(m)$ described in Eq. (35) can be approximated by,

$$z(m) = C_1 m + C_2 m^2 \quad (36)$$

where C_1 and C_2 are empirical constants. Substituting Eqs. (34) and (36) into Eq. (33) yields

$$R_s(m) = \frac{C_1 m + C_2 m^2}{k\{A_{01}[1 - ((C_1 m + C_2 m^2)/r_0)][1 - ((C_1 m + C_2 m^2)/h_0)] + A_{00}[1 - ((C_1 m + C_2 m^2)/r_0)]^2\}} \quad (37)$$

where $A_{00} = \pi r_0^2$ and $A_{01} = 2\pi r_0 h_0$. The constants, C_1 and C_2 are obtained by solving Eq. (35) over the range of m values in the model and the resulting "m, z" data pairs are fit to Eq. (36) to define C_1 and C_2. Eq. (37) is used to define R_s in Eqs. (29) and (30), allowing explicit description of the change in heat flow due to a contracting cylindrical geometry.

4. Results and discussion

The objective of this study was to construct the liquidus curve for frozen multicomponent solutions to accurately

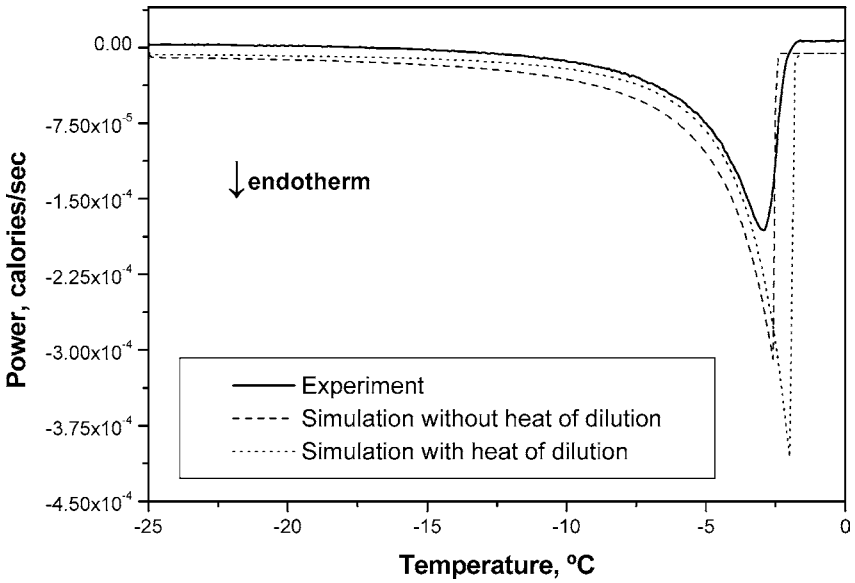

Fig. 2. Comparison between experiment and theory with and without the effect of heat of dilution. The melt endotherm was simulated for a 5 mg sample of 30% (w/v) sucrose at 0.2 °C/min using K_f =2.6, R = 541 cal^{-1} °C s, and T_{r_0} = −25 °C. The heat of dilution for a 30% (w/v) sucrose solution is 54 and 7 cal/g at −25 °C and at the end of melting, respectively. The heat of dilution at the end of melting is much smaller for less concentrated sucrose solutions (0.25 cal/g for 5% (w/v) sucrose). Despite the higher value at −25 °C, the heat of dilution does not qualitatively affect the shape of the endotherm when compared to the endotherm simulated without the effect of the heat of dilution as observed in figure. The effect of temperature on the heat of fusion is given by $\Delta C_p(T - T_m)$ and is 12.5 cal/g at −25 °C, which is smaller than the contribution of the heat of dilution to the total heat. Therefore, the effect of temperature on the heat of fusion was ignored in the simulation of the melt endotherm.

define the composition of the freeze-concentrate. To achieve that objective, we first set out to identify the feature of a DSC melt endotherm that most correctly reflected the end of the melt in a frozen solution.

4.1. Comparison of simulated melt endotherms from Gray's theory with experiment

Gray's theory for melting in one-component systems was extended to multicomponent systems to simulate the DSC melt endotherm. A comparison of the experimental and simulated melt endotherms for 30% (w/v) sucrose shows good agreement in the "peak smearing" region of the endotherms (Fig. 2). However, a difference in the recovery of the DSC power from the endotherm peak to the baseline is observed when simulated endotherms are compared with experiment. In the simulation that includes the heat of dilution, the peak temperature, T_{peak}, is shifted by +0.6 °C relative to the experimental value. Further, in both simulations, the endotherm is deeper and returns to the baseline within a 0.4–0.6 °C range in temperature, whereas the recovery of the signal from peak to baseline takes longer (+1.2 °C) experimentally.

It appears that even after the peak of the melt endotherm, there is considerable demand for heat, which suggests that the melting of ice is not complete at the peak. However, the conclusion from Gray's theory is that once all the ice has melted, the signal rapidly returns to baseline. Based on Gray's theory, the differential equation governing the time dependence of $(T_s - T_r)$ may be solved in closed form to obtain an equation that describes the recovery of the DSC signal from the peak to the baseline:

$$T_s - T_r = (T_s - T_r)_{max} \exp\left(-\frac{t}{RC_s}\right) \quad (38)$$

Using an example of a 5 mg sample of pure ice where R_T = 541 cal^{-1} °C s and C_s = 0.0174 cal/°C, Eq. (38) predicts that the signal is less than 1% of the maximum within a temperature of 0.14 °C from the peak in reference temperature at a scan rate of 0.2 °C/min versus 0.73 ± 0.02 °C as observed experimentally.

4.1.1. Calculation of thermal resistance for experimental and simulated endotherms

Thermal resistances, R_T, R, and R_s(m), were calculated for experimental and simulated endotherms. R_T values calculated from experimental peak widths using Eq. (11) were found to be remarkably similar even with a doubling of sample mass (Table 1). Additionally, R_T values[1] increased with an increase in the heating rate. This increase in apparent resistance is due to peak broadening in the data. It is likely that a thermal lag in the sample rather than a change in the resistance accounted for the peak broadening. Alternatively, Eq. (38) allows for the calculation of resistance based solely on the re-

[1] R_T was calculated using Eq. (11) after experimental determination of the width of the melt endotherm for different masses of pure ice (3–10 mg) at different heating rates (0.2–2.0 °C/min). An average value of R_T = 541 cal^{-1} °C s was used in the simulation of the endotherms.

Table 1
Comparison of thermal resistances, R_T, R, and $R_s(m)$ in experimental and simulated melt endotherms

Sample/heating rate	Experiment		Simulation using the HTD model using R_0 = 500 cal^{-1} °C s	
	R_T (Eq. (11)) (cal^{-1} °C s)	R (Eq. (38)) (cal^{-1} °C s)	$R_s(m)$ (Eq. (37)) at $T_{50\%\,melting}$	$R_s(m)$ (Eq. (37)) at T_{peak}
Ice: 5 mg				
0.2 °C/min	644 (133)[a]	548 (145)	93	195
2.0 °C/min	726 (148)	1034 (224)	93	216
Ice: 10 mg				
0.2 °C/min	585 (81)	1785 (711)	129	183
2.0 °C/min	734 (43)	1685 (272)	129	184

[a] Values in parenthesis are standard deviations.

turn of the peak to baseline, which according to Gray's theory occurs only after all melting has occurred. The resistance values calculated from experimental endotherms using Eq. (38) are, in general, higher than those calculated using Eq. (11), particularly for the larger sample mass. Using Eq. (37) from the Heterogeneous Temperature Distribution (HTD) model, the sample thermal resistance, $R_s(m)$, was calculated at the peak and also when 50% of the sample has melted. $R_s(m)$ values increase only slightly with an increase in sample mass, which explain the similarity in the R_T values we observe in Table 1. Also, $R_s(m)$ values at both T_{peak} and at the end of 50% melting, are smaller than R_T values by about 500 cal^{-1} °C s, confirming our use of R_0 = 500 cal^{-1} °C s for simulations here. Simulations using the HTD model show that the sample resistances, $R_s(m)$ increased with melting and continue to increase even beyond the peak (Fig. 3). This also suggests that the melting is not complete at the endotherm peak.

4.1.2. Recovery of peak signal to baseline: experiment versus simulation

Gray's theory predicts that the peak recovery to the baseline should be almost instantaneous, a phenomenon which is never observed experimentally. Our simulations of the endotherm for frozen sucrose:water systems using Gray's theory exhibited a quick return to the baseline that was insensitive to large changes in resistance (Fig. 2 and Table 2). However, the experimental signal recovery to the baseline was much longer (+0.7–5.0 s) than for the simulated endotherm. Therefore, we conclude that the homogeneous temperature model is insufficient. The demand for heat exceeds that which is predicted by Gray's theory, which assumes a homogeneous temperature distribution in the sample. Since heat must flow within the melted sample, temperature gradients must exist. It appears that these gradients are significant as seen from the melt endotherm obtained from experiment (Fig. 2) and from the recovery of the peak signal to the baseline (Table 2).

4.1.3. Comparison of simulated melt endotherms from HTD model with experiment

When Gray's theory is modified to include a heterogeneous temperature distribution (HTD model) within the sample during melting, the simulated melt endotherms show a better agreement with the return to the baseline data obtained from experiment than those obtained using extended Gray's

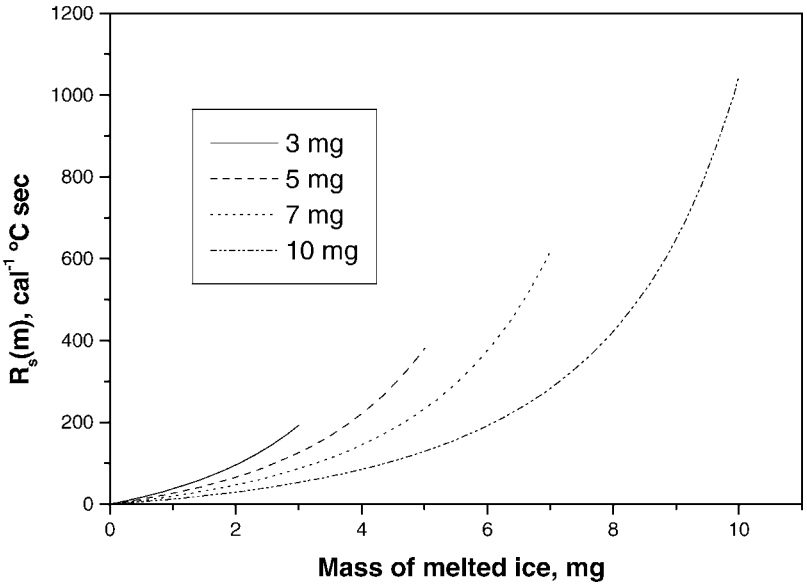

Fig. 3. Comparison of sample thermal resistance, $R_s(m)$ (cal^{-1} °C s) calculated from simulated melt endotherms of ice (3–10 mg) at 0.2 °C/min using Eq. (37).

Table 2
Comparison of the recovery of the peak signal to the baseline in experimental and simulated melt endotherms

Sample/heating rate	Experiment	Simulation (Gray's theory)	Simulation (HTD)	
	°C return to baseline from peak	°C return to baseline from peak	°C return to baseline = 200 from peak, R_0	°C return to baseline = 500 from peak, R_0
Ice: 5 mg		R_T = 500[b]		
0.2 °C/min	0.73 (0.02)[a]	0.06	0.50	0.50
2.0 °C/min	3.41 (0.22)	0.08	1.70	2.25
Ice: 10 mg		R_T = 1500[b]		
0.2 °C/min	1.25 (0.16)	0.08	0.85	0.95
2.0 °C/min	5.14 (0.54)	0.12	3.25	4.00

[a] Values in parenthesis are standard deviations.
[b] The recovery of the peak signal to the baseline exhibited low sensitivity to small changes in R_T. Therefore, a lower R_T value of 500 cal^{-1} °C s and a higher R_T value of 1500 cal^{-1} °C s were chosen to observe differences in peak signal recovery to the baseline.

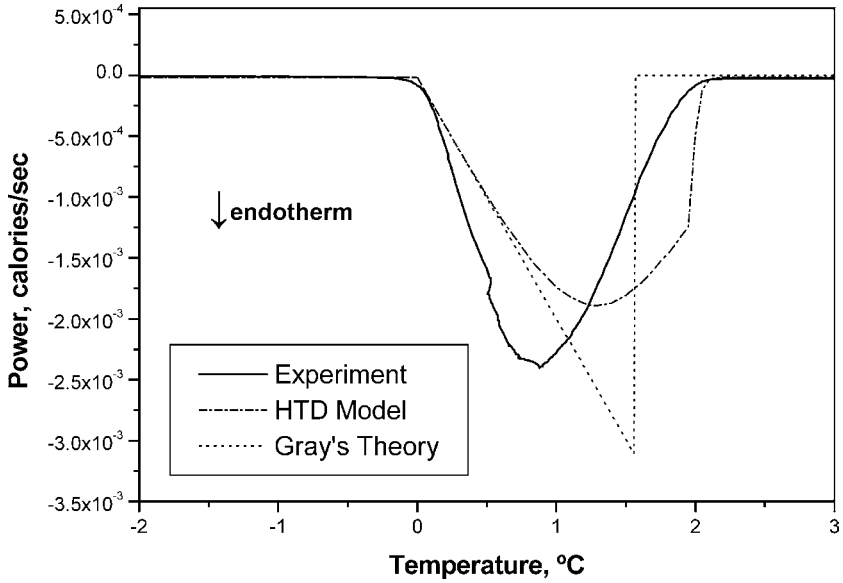

Fig. 4. A comparison of the melt endotherms for 10 mg water at a heating rate = 0.2 °C/min sample obtained from DSC experiment and from simulation using Gray's theory at R = 500 cal^{-1} °C s and the Heterogeneous temperature distribution model at R_0 = 500 cal^{-1} °C s. In the three examples shown above, the area of the endotherm is always the same.

theory (Table 2). In addition, the melt endotherm simulated using the HTD model exhibits a peak shape and a delayed recovery similar to the experimental endotherm (Fig. 4). The amount of ice melted at the peak of the endotherm was also calculated (Table 3). Melting is not complete at the peak, irrespective of the value of R_0. However, the percentage of ice melted at the peak increases with decreasing sample mass and with an increase in R_0. For 3 mg sample mass, 93% of ice is melted at the peak in an endotherm generated using R_0 = 500 cal^{-1} °C s when compared to 77% of ice melted at the peak in an endotherm generated using R_0 = 200 cal^{-1} °C s (Table 3). It appears that a higher R_0 results in a more uniform temperature distribution across the sample, and a more Gray's theory-like endotherm. However, the amount of ice melted at the peak is much lower at higher sample masses. The HTD model resolves total thermal resistance, R_T, into a thermal resistance across the DSC furnace:sample pan, R_0, and a sample thermal resistance, $R_s(m)$ (Fig. 3). The HTD model clearly predicts that the melting continues beyond the peak and a delayed recovery from peak to the baseline is

Table 3
Percentage of total ice melted at the endotherm peak using HTD model

Mass of ice (mg)	R_0 = 200 cal^{-1} °C s		R_0 = 500 cal^{-1} °C s	
	Mass of ice melted (mg)	Ice melted (%)	Mass of ice melted (mg)	Ice melted (%)
3	2.3	77	2.8	93
5	2.8	56	3.9	78
7	3.4	49	4.6	66
10	4.5	45	5.9	59

observed, similar to experimental observations and contrary to what is predicted using Gray's theory. Additional results from the HTD model are included in Section 4.2.

4.2. Simulation of sample and instrumental effects on melt endotherms from the HTD model

Further evaluations were carried out to determine whether the peak shape features observed in a series of experimental endotherms could be predicted using various instrumental and sample parameters. Using the theory developed in Section 3.2, we evaluated the effect of sample geometry, thermal resistance across the DSC furnace and sample pan, heating rate, and sample mass on the shape of the melt endotherm and the position of the endotherm peak, T_{peak}, and, the temperature at which the signal returned to baseline, T_{offset} (Fig. 5a–d).

The effect of sample geometry on the shape of the melt endotherm and the position of T_{peak} and T_{offset} is shown in Fig. 5a. A conventional sample pan geometry yields a fairly broad peak as observed experimentally. It is not until the sample radius is double the conventional shape that the simulated endotherm approaches Gray's prediction of peak shape. Since the sample is flatter, there is less heterogeneity in the temperature distribution, and melting is complete at the peak under these extreme conditions. However, using the conventional

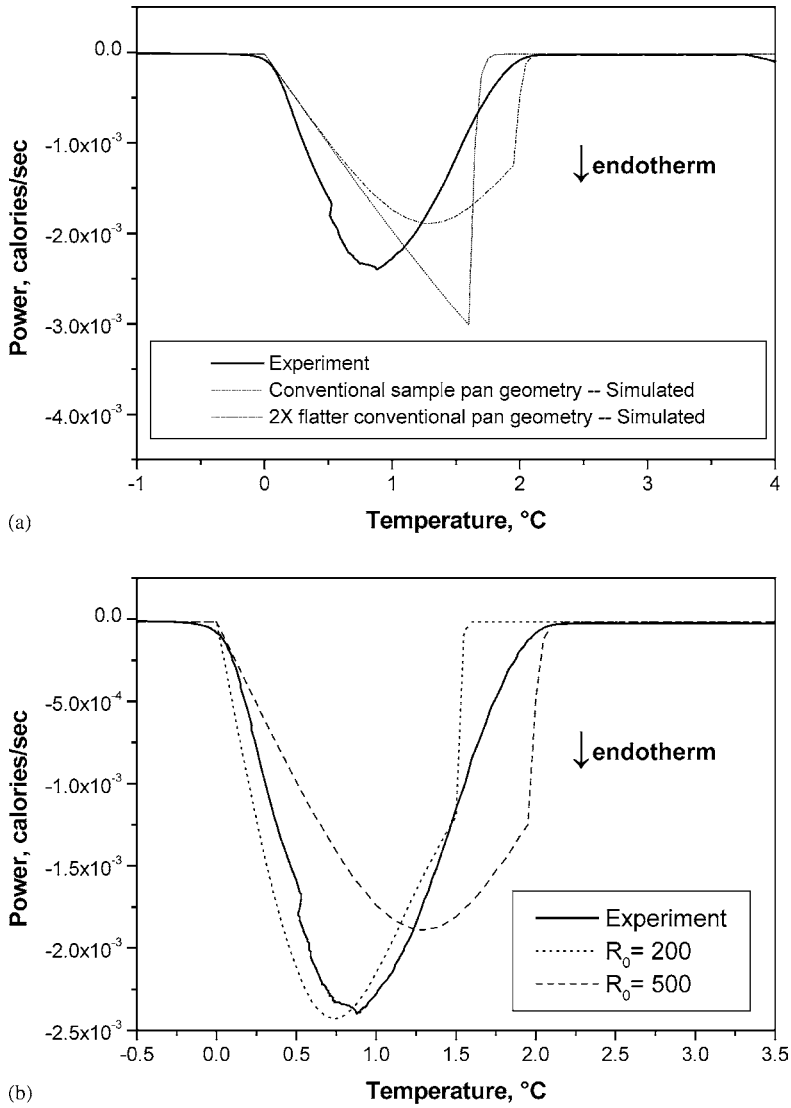

Fig. 5. (a) Effect of sample geometry on the shape of the melt endotherm of 10 mg ice at R_0 = 500 cal^{-1} °C s at a heating rate of 0.2 °C/min. (b) Effect of thermal resistance across the DSC furnace and the sample pan, R_0, on the shape of the melt endotherm of 10 mg ice at a heating rate of 0.2 °C/min. R_0 values of 200 and 500 cal^{-1} °C s were used as the simulated endotherms generated using these values showed a reasonable agreement with experimental peak and offset data, respectively. (c) Effect of heating rate on the shape of the melt endotherm of 10 mg ice at R_0 = 500 cal^{-1} °C s. "E" and "S" represent the experimental and simulated melt endotherms, respectively. (d) Effect of the sample mass on the shape of the melt endotherm of ice at R_0 = 500 cal^{-1} °C s and a heating rate of 0.2 °C/min. "E" and "S" represent the experimental and simulated melt endotherms, respectively.

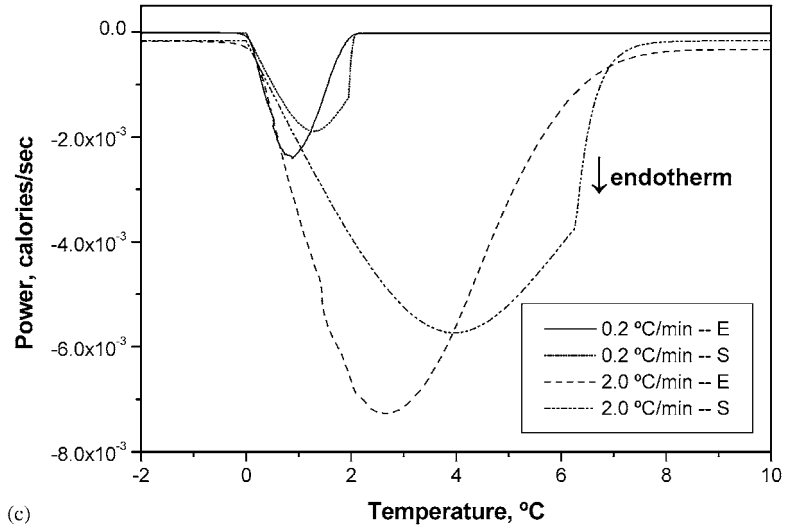

(c)

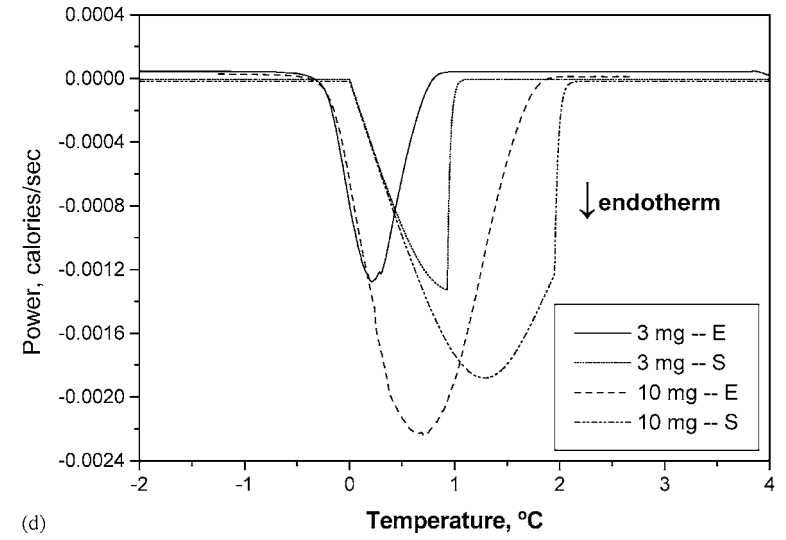

(d)

Fig. 5. (*Continued*).

sample pan, it is observed that melting is not complete at the peak. One may suggest the use of very small samples. However, we have found that 3 mg aqueous samples do not spread evenly over the bottom of the pan resulting in poorly reproducible endotherms.

A thermal resistance value of 500 $cal^{-1}\,^{\circ}C\,s$ predicts a peak width similar to the experimental endotherm (Fig. 5b), whereas, a lower thermal resistance (200 $cal^{-1}\,^{\circ}C\,s$) predicts a peak temperature closer to the experimental value. Fig. 5c shows an increase in T_{peak}, T_{offset}, and the peak area with an increase in the heating rate for both simulated and experimental melt endotherms. Similarly, the simulated T_{peak}, T_{offset}, and the peak area increase with sample size as seen experimentally. Thus, the HTD predicts the same effect of heating rate and sample mass that is seen experimentally. Furthermore, the HTD model shows that the end of melting in a one-component system (ice) can occur beyond the peak temperature in a melt endotherm.

4.3. Determination of freezing point depression from DSC

As stated earlier, our interest lies in the determination of the freezing point depression or end of melting in a frozen solution so that the composition of the freeze-concentrate can be defined. Conventionally, T_{peak} is used to denote T_{melt}. However, since the results described above indicate that T_{peak} is generally not the feature associated with the end of melting we analyzed both the use of the T_{peak}, and the T_{offset}, the return to the baseline as markers for the end of melting. Fig. 6 shows a comparison of the theoretically predicted end of melting, T_m, with the experimental T_{offset} and T_{peak}. T_m obtained from simulation shows better agreement with experimental T_{offset} than with experimental T_{peak} values over a range of heating rates (0.2–2.0 °C/min). However, there is a strong heating rate dependency. It is obvious that an extrapolation to a zero heating rate is required to obtain freezing point depression

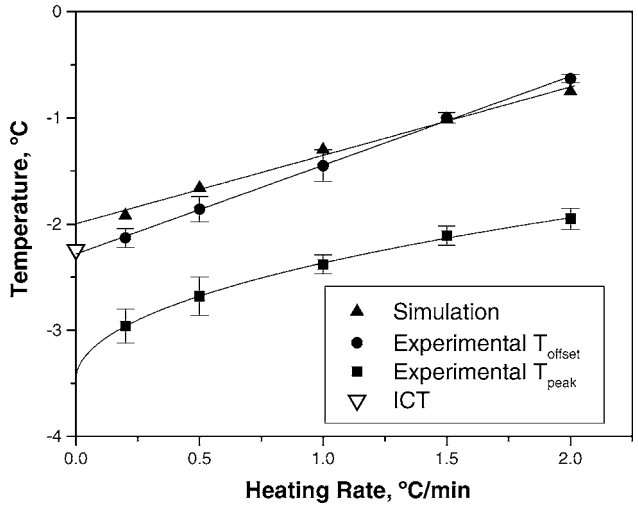

Fig. 6. Comparison of experimental offset and peak data with simulated data for 30% (w/v) sucrose (5 mg). The simulated data points were obtained from a melt endotherm simulated for a 5 mg sample of 30% (w/v) sucrose using K_f = 2.6, R = 541 cal^{-1} °C s, and T_{r_0} = −25 °C.

values that agree with the International Critical Tables (ICT) data. The freezing point depression numbers from the ICT are not calorimetrically obtained values. However, to this day, the ICT data are accepted as the "gold standard" for equilibrium freezing point depression values and use in the construction of liquidus curves of carbohydrate–water systems.

Using experimental and simulated scans, an extrapolation of either T_{peak} or T_{offset} to a zero scan rate predicted a T_{melt} of zero for pure ice, irrespective of the sample mass or the thermal resistance (data not shown). The convergence of all extrapolated values to the true value argues further for the extrapolation of DSC data to obtain better estimates of true equilibrium values.

The heating rate dependence of the experimental offset temperatures during the experiment was studied in more detail (Fig. 7). The offset temperatures of water and concentrated sucrose solutions (≥30%, w/v) exhibit different dependencies on the heating rate. A well-defined curvature appears at much lower heating rates (0.05–0.2 °C/min, data not shown) for water and more dilute sucrose solutions (≤30%, w/v). The analysis of the experimental melt endotherms for water samples and for sucrose solutions (≤30%, w/v) show that an extrapolation function, which is quadratic in the square root of scan rate, best fits the data (Fig. 7). On the other hand, a linear dependency on the heating rate is observed for more concentrated sucrose solutions (≥30%, w/v). In addition, simulations of aqueous sucrose endotherms show exactly the same behavior (scan rate dependency for less versus more concentrated sucrose solutions) as the experimental results. Such analysis has implications in the accurate determination of equilibrium freezing point determination and the calculation of the freeze-concentrate composition at different sub-zero temperatures.

A comparison of the extrapolated offset and peak temperatures with osmometry data and literature values (from ICT) shows that the sample mass dependency and the heating rate dependency appear to dissipate upon an extrapolation of T_{offset} to a zero scan rate (Table 4). Reasonable agreement is seen between extrapolated T_{offset} DSC data, the literature values and the osmometry data.

4.4. Determination of composition of the sucrose:water freeze-concentrate using the liquidus curve

Extrapolated T_{offset} and T_{peak} values from Table 4 were used to construct the sucrose:water liquidus curve. The

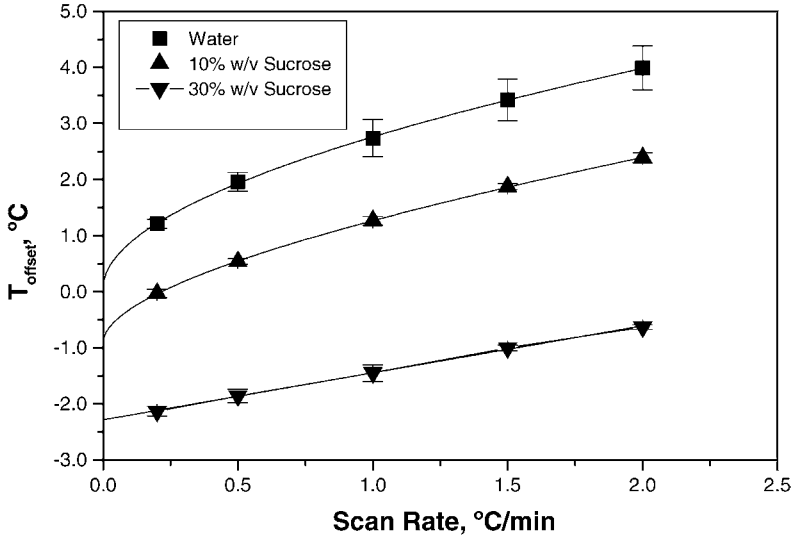

Fig. 7. Comparison of the heating rate dependency of the experimental offset temperature for pure water, and 10% (w/v) and 30% (w/v) sucrose (5 mg). The results obtained from the simulations (data not shown) are the same as those obtained from the experiment (shown above).

Table 4
Comparison of extrapolated offset and peak temperature data with osmometry data and ICT values

Sucrose (%, w/v)	Sample size (mg)	Extrapolated T_{offset} (°C)	Extrapolated T_{peak} (°C)	Osmometry (°C)	Literature values (°C[a])
5	5	−0l5	−0l5	−0.3 (157.5 mOsm)	−0.3
10	3	−0l8 (0.0)[b]	−1l0 (0.2)	−0.6 (327 mOsm)	−0.6
	5	−0l9 (0.2)	−0l8 (0.1)		
	7	−1l0 (0.3)	−0l8 (0.1)		
	10	−0l8 (0.1)	−0l7 (0.1)		
Mean[c]		−0l9 (0.2)	−0l8 (0.1)		
20	3	−1l8 (0.2)	−3l1 (0.4)	−1.4 (766.0 mOsm)	−1.3
	5	−1l4 (0.0)	−1l8 (0.2)		
	7	−1l9 (0.0)	−2l3 (0.1)		
	10	−1l7 (0.1)	−1l8 (0.1)		
Mean		−1l7 (0.3)	−2l0 (0.3)		
30	3	−2l8 (0.4)	−4l3 (0.2)	−2.4 (1289.8 mOsm)	−2.2
	5	−2l4 (0.2)	−3l5 (0.2)		
	7	−2l0 (0.1)	−3l0 (0.1)		
	10	−2l1 (0.1)	−3l0 (0.2)		
Mean		−2l1 (0.2)	−3l2 (0.3)		
60	3	−10l8 (1.2)	−11l6 (1.1)	–	−6.9
	5	−8l6 (0.5)	−9l7 (0.7)		
	7	−7l9 (0.6)	−9l2 (0.5)		
	10	−7l4 (0.3)	−8l7 (0.4)		
Mean		−7l9 (0.7)	−9l2 (0.7)		

[a] International Critical Tables of Numerical Data, Physics, Chemistry, and Technology. Vol. IV, 1928, data pooled from six sources, which differ by no more than ±5%.
[b] Values in parenthesis represent standard deviations.
[c] The values represent mean of the extrapolated offset or peak temperatures for sample sizes 5–10 mg.

liquidus curve generated using extrapolated T_{offset} (Fig. 8) agrees much better with the liquidus curve from ICT than does the one generated using extrapolated T_{peak} data.

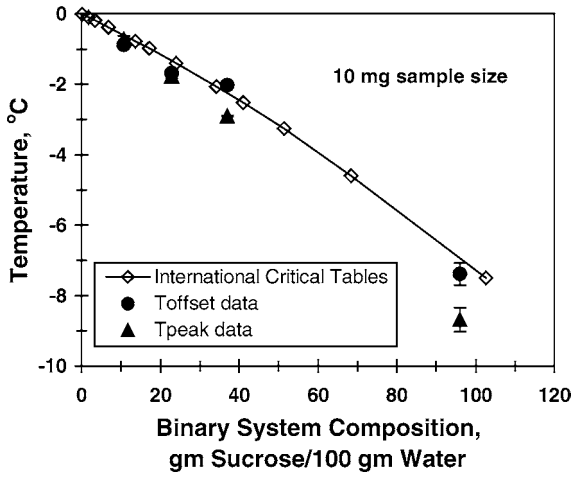

Fig. 8. A comparison of experimentally determined liquidus curves using DSC with the liquidus curve from the International Critical Tables based on extrapolation of experimental T_{peak} and T_{offset} to a zero scan rate.

The effect of a lower freezing point depression on accuracy in determination of composition of the freeze-concentrate is shown in Table 5. The composition of the freeze-concentrate at −5 °C was calculated for a multicomponent system containing 2% (w/v) sucrose, 5 μg/mL enzyme, and 0.05 M buffer. Additional experiments (data not shown) showed that that the enzyme and the buffer exhibited no effect on the freezing point depression of water. Thus, a liquidus curve for a sucrose-water system could be used to perform such calculations. The increase in concentration upon freezing has been calculated using ICT as well as extrapolated T_{offset} and T_{peak}. For the T_{offset} and T_{peak} data, the ranges of values shown represent the values obtained using DSC data for sample masses varying between 5 and 10 mg. Table 5 shows the range of values one can obtain to define the composition of a freeze-concentrate. Inaccurate determination of the freeze-concentrate composition can lead to misinterpretations in analysis of stability data of drugs labile to freezing. It is obvious based on experimental data and theory that the use of the T_{offset} data results in a freeze-concentrate composition that shows a better agreement with the composition defined by the ICT.

Table 5
Comparison of the composition of the freeze-concentrate at −5 °C for an enzyme:sucrose:buffer solution based on the sucrose–water phase diagram from DSC T_{offset} and T_{peak} data and the International Critical Tables

	Concentration prior to freezing	Increase in concentration after freezing based on		
		International Critical Tables (ICT)	Extrapolated T_{peak}	Extrapolated T_{offset}
X-fold increase in concentration after freezing at −5 °C		25	18.7[a]–20.4[b]	21.5[a]–23.5[b]
Sucrose (%, w/v)	2	50	37.3–40.8	43.0–47.0
Enzyme (5 μg/mL)	5	125	93.5–102.6	107.5–117.5
Buffer (0.05 M)	0.05	1.25	0.94–1.02	1.08–1.18

[a] The lower end of the range represents values of composition obtained using liquidus curve generated from melting of 5 mg DSC sample.
[b] The upper end of the range represents values of composition obtained using liquidus curve generated from melting of 10 mg DSC sample.

5. Conclusions

Our work on frozen sucrose solutions has shown that the use of a randomly chosen heating rate and sample mass in DSC studies results in freezing point depression values that do not agree with the gold standard, i.e., the International Critical Tables (ICT). Using freezing point osmometry, we have determined that the ICT values are accurate even though these measurements were performed prior to the development of calorimetric methods in the late 19th and early 20th centuries. Mathematical modeling proved to be of significant use in the determination of the most suitable marker for the end of melting (T_{peak} versus T_{offset}). The simulations based on our simple one- and two-component models were not exactly in agreement with the experimental endotherms, but exhibited the same trends as observed from experiment. A further refinement of the models may in fact result in simulations that are in better agreement with the experiment. The role of thermal resistance in the determination of the position of T_{peak}, T_{offset}, recovery of the peak to the baseline and the shape of the endotherm was studied using the HTD model. Further, the sample mass and geometry are intricately linked to the thermal resistance during melting and also affect the temperature distribution in a melting sample with a contracting cylindrical geometry as observed from the one-component modeling. From experiments and modeling studies on frozen one- and two-component solutions, we have shown that the extrapolated offset temperature is a better indicator of the freezing point depression than the extrapolated peak temperature. The use of extrapolated T_{offset} results in reliable values of freeze-concentration that are in good agreement with values calculated using the International Critical Tables. In addition, extrapolation to a zero scan rate is a better way of defining the equilibrium freezing point on a liquidus curve than without any extrapolation, and leads to a reliable determination of the composition of freeze-concentrates.

Acknowledgements

The authors thank Dr. Evgenyi Y. Shalaev, Pfizer Inc. for his helpful discussions. The support of the National Science Foundation Center for Pharmaceutical Center for Pharmaceutical Processing Research (NSF CPPR) and Parenteral Drug Association (PDA) Foundation for Bakul Bhatnagar and Rhone-Poulenc France for Stephane Cardon is acknowledged. The authors thank Avani Patel for assistance with osmometry measurements.

References

[1] M.J. Pikal, in: J. Swarbick, J.C. Boylan (Eds.), Encyclopedia of Pharmaceutical Technology, Marcel Dekker, New York, 2001, pp. 1299–1326.
[2] K.-I. Izutsu, S. Kojima, Pharm. Res. 17 (2000) 1316.
[3] A.M. Peres, E.A. Macedo, Fluid Phase Equilib. 123 (1996) 71.
[4] A.M. Peres, E.A. Macedo, Fluid Phase Equilib. 139 (1997) 47.
[5] G.D. Fullerton, C.R. Keener, I.L. Cameron, J. Biochem. Biophys. Methods 29 (1994) 217.
[6] F.E. Young, F.T. Jones, J. Phys. Colloid Chem. 53 (1949) 1334.
[7] C.P. Pickering, Ber. Deut. Chem. Ges. 24 (1891) 3328.
[8] F.M. Raoult, Cr. Hebd. Acad. Sci. 125 (1897) 751.
[9] T. Ewan, Z. Phys. Chem. 31 (1899) 22.
[10] E.W. Washburn, International Critical Tables of Numerical Data, Physics, Chemistry and Technology, vol. IV, McGraw-Hill, New York, 1928, p. 263.
[11] G. Steinbach, Sci. Technol. Froid 1 (1977) 53.
[12] B. Luyet, D. Rasmussen, Biodynamica 10 (1968) 167.
[13] A.P. MacKenzie, Philos. Trans. R. Soc. Lond. B: Biol. Sci. 278 (1977) 167.
[14] A.N. Kanev, V.I. Kosyakov, D.V. Malakhov, E.Y. Shalaev, Izv. Sib. Otd. Akad. Nauk SSSR, Ser. Khim. Nauk 2 (1989) 11.
[15] S. Ablett, M.J. Izzard, P.J. Lillford, J. Chem. Soc., Faraday Trans. 88 (1992) 789.
[16] G. Blond, D. Simatos, M. Catte, C.G. Dussap, J.B. Gros, Carbohydr. Res. 298 (1997) 139.
[17] G.M. Wang, A.D.J. Haymet, J. Phys. Chem. B 102 (1998) 5341.
[18] M. Schoenitz, A. Navrotsky, K. Leinenweber, Phys. Chem. Miner. 27 (2000) 604.
[19] C.P. Tan, Y.B.C. Man, Phytochem. Anal. 13 (2002) 129.
[20] R.H.M. Hatley, A. Mant, Int. J. Biol. Macromol. 15 (1993) 227.
[21] L.M. Her, S.L. Nail, Pharm. Res. 11 (1994) 54.
[22] E.Y. Shalaev, F. Franks, J. Chem. Soc., Faraday Trans. 91 (1995) 1511.
[23] Y.H. Roos, J. Therm. Anal. 48 (1997) 535.
[24] V.T. Popa, E. Segal, J. Therm. Anal. Calorim. 69 (2002) 149.
[25] G. Wang, I.R. Harrison, Thermochim. Acta 230 (1993) 309.
[26] G. Wang, I.R. Harrison, Thermochim. Acta 246 (1994) 153.
[27] G. Wang, I.R. Harrison, Thermochim. Acta 231 (1994) 203.
[28] A.P. Gray, in: R.S. Porter, J.F. Johnson (Eds.), Analytical Calorimetry, 1968, pp. 209–218.